Quasi-Static Derived Physically Expressive Circuit Model for Lossy Integrated RF Passives

Hai Hu, Kai Yang, Ke-Li Wu, *Senior Member, IEEE*, and Wen-Yan Yin, *Senior Member, IEEE*

***Abstract*—This paper presents a novel approach for *deriving* a physically meaningful circuit model for integrated RF lossy passives such as spiral inductors on a silicon substrate. The approach starts from a quasi-static partial element equivalent circuit (PEEC) model. The concept of complex inductance and capacitance is introduced to uniformly deal with the conductor and dielectric losses. Basic $Y-\Delta$ network transformation is used to "absorb" the insignificant internal nodes of the original PEEC network and to reduce the order of the circuit model. The physically expressive circuit model given here can be very concise while preserving the major physical meanings and attributes of the original circuit layout. A low-temperature co-fired ceramic bandpass filter and two practical inductors fabricated using a 0.18-μm CMOS process are studied by the model to demonstrate the validity of this new approach. Furthermore, the stability condition of the model is also discussed.**

***Index Terms*—Equivalent circuits, low-temperature co-fired ceramic (LTCC), microwave circuits, model-order reduction, RF integrated circuit (RFIC).**

I. Introduction

INTEGRATED RF passive components, either in silicon-based system-on-chip (SoC) or in ceramic/organic substrate-based system-in-package (SiP), are the key building elements that construct a single-chip monolithic functional system. New configurations and modeling techniques for the passives in an RF integrated system have been drawing a great deal of attention [1]–[4]. Needless to say, the characteristics of integrated RF passive components, e.g., the Q value of an inductor, will decisively determine the overall performance of the system. With the increase of the operating frequency, how to represent the inevitable parasitic effects and the loss properties of both substrate and conductors becomes one of the major challenges to the designers. Even though the modern full-wave electromagnetic simulation software packages are more powerful than ever before, they still could not provide good intuitive insights of those parasitic effects and a good physically expressive circuit representation, not to mention the long computation time for a large-scale system. In fact, a lot of efforts have been devoted to the electromagnetic simulation and model extraction methodologies for the integrated passives in various of substrates. The studies worth mentioning include [5] and [6], which intend to provide a simple computer-aided design (CAD) tool for extracting either capacitance or inductance values, respectively.

It is well understood that the performance of integrated RF passives, such as the inductors integrated on a silicon substrate, severely suffer from the losses associated with the conductor and the substrate in the gigahertz frequency range. Several previous studies have addressed these loss effects. In [7], Niknejad and Meyer analyzed electrical substrate loss, and presented a computationally efficient algorithm for designing and optimizing spiral inductors [8]. Cao *et al.* studied the loss effect at the high-frequency range and proposed a frequency-independent ladder *RLC* circuit to model the RF spiral inductors in [9]. Reference [10] classified the lossy parasitics into different mechanisms, such as the skin effect and eddy current, and suggested the use of finer mesh segments in modeling the loss. In addition, Weisshaar *et al.* proposed the idea of the "complex current image" in [11], which allows an image current located at a complex distance to account for the eddy-current effect. All these measures are effective to a certain extent; they were attempting to use a simple and predefined circuit to model the loss effects or to use a complicated *RLC* network to represent an RF circuit layout. Nevertheless, there are no efficient and generic methods that can *derive* a succinct physically meaningful circuit model from the given layout of a lossy RF integrated passive circuit.

The partial element equivalent circuit (PEEC) [12] technique is based on the mixed-potential integral equation (MPIE). The PEEC, which converts a circuit layout into a lumped *RLC* element coupled network, has been widely used in the modeling of integrated passives. For example, [13] proposed a scalable model for a spiral inductor on a lossy silicon substrate using an enhanced PEEC method. Unfortunately, the number of nodes and the number of components in the generated network are usually excessively large, which make the traditional SPICE-like circuit solvers extremely slow in running and is prohibitively difficult in revealing the physical insights. Therefore, researchers have been searching for more effective means that can reduce the circuit model order to accelerate circuit analysis [14]–[16] from the system transfer function point of view. Frequently, one also needs to find an appropriate circuit representation of a passive circuit from both physical intuition and system response [17], [18]. Recently, a systematic approach to derive a quasi-static physically meaningful circuit model with a specified order of accuracy for a lossless integrated passive was

Manuscript received October 4, 2007; revised May 6, 2008. First published July 15, 2008; last published August 8, 2008 (projected). This work was supported by the Research Grants Council of the Hong Kong Special Administrative Region under Grant 2150499.

H. Hu, K. Yang, and K.-L. Wu are with the Department of Electronic Engineering, The Chinese University of Hong Kong, Shatin, Hong Kong (e-mail: hhu@ee.cuhk.edu.hk; kyang@ee.cuhk.edu.hk; klwu@ee.cuhk.edu.hk).

W.-Y. Yin is with the Center for Microwave and RF Technologies, Shanghai Jiao Tong University, Shanghai 200240, China (e-mail: wyyin@sjtu.edu.cn).

Color versions of one or more of the figures in this paper are available online at http://ieeexplore.ieee.org.

Digital Object Identifier 10.1109/TMTT.2008.927307

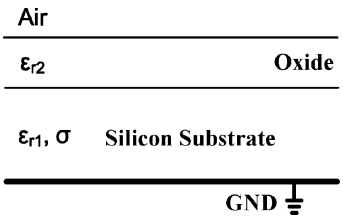

Fig. 1. Substrate of a typical CMOS IC.

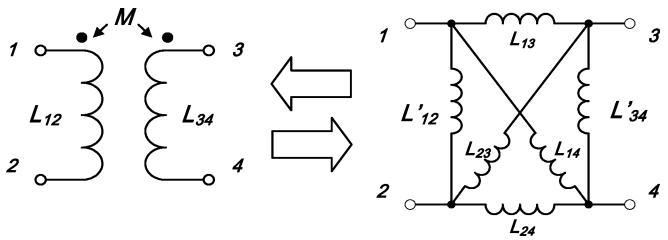

Fig. 2. Converting mutual inductances into self-inductances.

proposed [19]. However, the quasi-static model is only for the lossless case and cannot be directly applied to many practical cases in which the losses are too significant to be ignored.

In this paper, the above derived physically expressive circuit (DPEC) model is extended to the lossy integrated passive circuit case. This extension is based on a uniform treatment of complex capacitances and inductances. The guideline of how to ensure the passivity of the DPEC model is also discussed. The case studies of a low-temperature co-fired ceramic (LTCC) bandpass filter and two vertical spiral inductors built on a silicon substrate are given to show the validity and effectiveness of the extended DPEC model. It can be seen that, in all the examples, the loss properties, such as Q values versus frequency, are very well preserved in the DPEC model. It is demonstrated that the extended DPEC model for lossy circuits can effectively retain the essences of a lossy integrated passive circuit.

II. Theory

A. Quasi-Static PEEC Circuit Model With Losses

The PEEC modeling starts by dividing a multilayer circuit structure into a number of capacitive and inductive meshes. The conductive loss is then incorporated in the complex numbered self-inductors and the dielectric loss is included in the complex numbered self capacitors.

The dielectric loss can be taken into account by including the complex dielectric constant $\varepsilon_r = \varepsilon_r'(1 - j\tan\delta)$ in the Green's functions that are associated to the substrate structure under consideration. A brief description of PEEC modeling can be found in [19].

Since the conductive loss is primarily determined by the skin-depth effect in RF frequency, a similar surface impedance model to that used in the method of moment [20] can be employed in the quasi-static PEEC modeling.

Since the quasi-static simplification is well known to be accurate enough for modeling RF integrated circuit (RFIC) and monolithic microwave integrated circuit (MMIC) devices, the quasi-static Green's functions are employed in this study. Due to the lossy nature of silicon, the potential Green's functions are complex. The vertical structure of a typical silicon-based integrated circuit (IC) is shown in Fig. 1. The spectral-domain potential Green's functions can be derived using transmission line theory [21].

An important step during the derivation of the DPEC model is to carefully convert all the mutual inductances between the inductive mesh elements in a PEEC model into a directly connected inductor network. A simple demonstrative example is shown in Fig. 2. The mutual inductance M between the self-inductor pair of L_{12} and L_{34} is equivalently transformed into four directly connected inductances, namely, L_{13}, L_{23}, L_{14}, and L_{24}, whereas L_{12} and L_{34} are modified by L_{12}' and L_{34}'.

The values for L_{13}, L_{23}, L_{14}, L_{24}, L_{12}', and L_{34}' can easily be obtained from the values of M , L_{12}, and L_{34} by circuit analysis. L_{12}' and L_{34}' in Fig. 2 are called main inductances, as they originate from the inductive meshes of a layout. L_{13}, L_{23}, L_{14}, and L_{24} are defined as inter-inductances, as they are generated from mutual inductance M, despite a similar nature to self-inductances. In general, inter-inductances are substantially larger than the main inductances.

A point that deserves mentioning here is that the conductive loss will only be associated with main inductors. Thus, no resistance should be associated to the inter-inductances after the mutual inductance is transformed to inter-inductances. This point is very important for preserving the passivity of a DPEC model.

B. DPEC Model

In order to incorporate the conductive loss and dielectric loss in a uniform manner, the concept of complex capacitance and complex inductance is introduced. The impedance of a complex inductor is expressed as

$$Z_L = j\omega L + R_L = j\omega(L - jR_L/\omega) = j\omega\tilde{L}_{\text{new}} \qquad (1)$$

where R_L is conductive loss of an inductive mesh, which is obtained by multiplying the surface impedance with the integration of the basis function over an inductive cell. Similarly, for a complex capacitor, one can define

$$Z_C = \frac{1}{(j\omega C + G_C)} = \frac{1}{j\omega(C - jG_C/\omega)} = \frac{1}{j\omega\tilde{C}_{\text{new}}} \qquad (2)$$

where G_C accounts for the dielectric loss, which is included in the Green's functions. Since the lossy elements in (1) and (2) are all frequency dependent, the resultant complex components also depend on frequency. Having incorporated the above-defined complex inductance and capacitance in a PEEC model, a complex valued network representation of the original lossy circuit layout can be obtained. Therefore, the next task is to reduce the order of the excessively large PEEC network and to derive a concise DPEC model.

The basic principle of the DPEC model is based on the Gaussian elimination or the $Y - \Delta$ transformation [19]. It says an N-node Y circuit can be transformed to an $(N - 1)$-node Δ circuit. For readers' convenience, the basic formula for the DPEC model is repeated here.

The adjacent admittances in the Δ circuit from the transformation can be calculated by

$$y_{mn} = \frac{y_m y_n}{Y_t} \tag{3}$$

where y_m and y_n are the admittances in the Y circuit, and Y_t is the total admittances connected to the node that has been reduced. Considering the generic case of y_m and y_n, which are in the form of a complex *LC* tank, (3) can be specifically expressed as

$$y_{mn} = j\omega\tilde{C}_e + \frac{1}{j\omega\tilde{L}_e} + \frac{1}{j\omega\tilde{L}'_e + 1/j\omega\tilde{C}'_e} \tag{4}$$

where

$$\tilde{C}_e = \frac{\tilde{C}_m\tilde{C}_n}{\tilde{C}_t}, \quad \tilde{L}_e = \frac{\tilde{L}_m\tilde{L}_n}{\tilde{L}_t} \tag{5}$$

$$\tilde{C}'_e = \frac{\tilde{C}_n\tilde{L}_t}{\tilde{L}_m} + \frac{\tilde{C}_m\tilde{L}_t}{\tilde{L}_n} - \frac{\tilde{C}_m\tilde{C}_n}{\tilde{C}_t} - \frac{\tilde{L}_t^2\tilde{C}_t}{\tilde{L}_m\tilde{L}_n}$$

$$\tilde{L}'_e = \left(\frac{\tilde{C}_n}{\tilde{L}_m\tilde{C}_t} + \frac{\tilde{C}_m}{\tilde{L}_n\tilde{C}_t} - \frac{\tilde{L}_t}{\tilde{L}_m\tilde{L}_n} - \frac{\tilde{C}_m\tilde{C}_n}{\tilde{L}_t\tilde{C}_t^2}\right)^{-1} \tag{6}$$

and $\tilde{L}_t$ and $\tilde{C}_t$ are the equivalent inductance and capacitance of the total admittance connected to the node that has been reduced.

Apparently, (4) cannot be restored to an admittance in the form of an *LC* tank without a legitimate treatment. In order to develop a recursive process, the third term in (4) needs to be converted to a complex capacitance before removing the next "removable" node such that

$$y^{(3)}_{mn} = \frac{1}{j\omega\tilde{L}'_e + 1/j\omega\tilde{C}'_e} = \frac{j\omega\tilde{C}'_e}{1 - \omega^2\tilde{L}_t\tilde{C}_t}. \tag{7}$$

The choice of the node that best satisfies the condition of $|\omega^2\tilde{L}_t\tilde{C}_t| \ll 1$ at each step of the process is critical for retaining the physical meanings of the circuit. That is to say, the node that gives the smallest value of $|\omega^2\tilde{L}_t\tilde{C}_t|$ at an iteration step will be "absorbed." The recursive iteration process is repeated until the values of $|\omega^2\tilde{L}_t\tilde{C}_t|$ for all the internal nodes are larger than a prescribed threshold value. Setting a threshold value, say, 0.15, is to ensure a smooth and nearly monotonous change of the component values in the frequency range of interest. Obviously, the DPEC topology is determined at the highest frequency of interest.

It should be mentioned that similar equations to (3)–(7) have been given in [19]. The differences are that here the inductance and capacitance are complex numbers and are frequency dependent in general.

C. Passivity of the DPEC Mode for Lossy Circuits

Since the original PEEC model network is passive, the passivity property of a DPEC model must be retained. In conducting $Y - \Delta$ circuit transformation, a positive imaginary part of some complex capacitances $\tilde{C}'_e$ can be found. Since their values are substantially large, these positive imaginary parts can be discarded without affecting the attributes of the DPEC model. However, special attention needs to be paid to the stability problem with inductance.

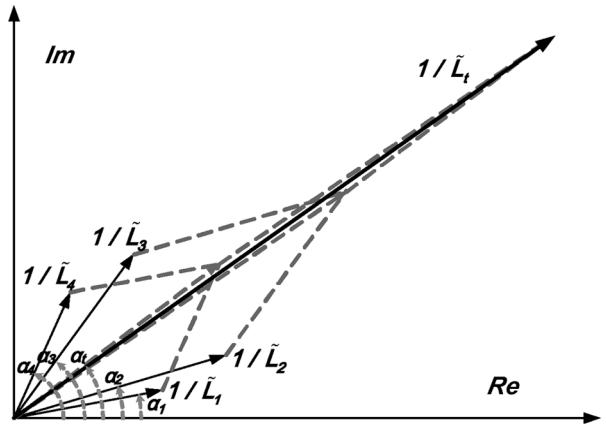

Fig. 3. Vector diagram of $1/\tilde{L}_t$. The angles for reciprocals of the complex inductances have been exaggerated in order to give a clearer sketch.

Assuming uniform meshes are used, a vector diagram can be employed to illustrate how the passivity of a DPEC model can be guaranteed if the inductive meshes are fine enough. As the main complex inductance can be written in an exponential form

$$\tilde{L} = L - j\frac{R_L}{\omega} = |\tilde{L}|e^{-j\alpha} \tag{8}$$

where $0 < \alpha < \pi/2$, the reciprocal of the total inductance $\tilde{L}_t$ in (5) can be expressed by

$$\frac{1}{\tilde{L}_t} = |1/\tilde{L}_1|e^{j\alpha_1} + |1/\tilde{L}_2|e^{j\alpha_2} + \cdots + |1/\tilde{L}_k|e^{j\alpha_k}. \tag{9}$$

The vector diagram for $1/\tilde{L}_t$ is shown in Fig. 3, where four adjacent inductances are considered. If $\alpha_{\min}$ and $\alpha_{\max}$ are the smallest and largest angles among $\alpha_1, \alpha_2, \ldots, \alpha_k$, respectively, we have $\alpha_{\min} < \alpha_t < \alpha_{\max}$. The new inductances $\tilde{L}_e$ between nodes n and m after $Y - \Delta$ circuit transformation can be expressed by

$$\tilde{L}_e = |\tilde{L}_e|e^{j\alpha_e} = \left|\frac{\tilde{L}_n\tilde{L}_m}{\tilde{L}_t}\right| e^{j(-\alpha_m - \alpha_n + \alpha_t)}. \tag{10}$$

whose complex angle α_e can be rewritten as

$$\begin{aligned}\alpha_e &= -\alpha_m - \alpha_n + \alpha_t < -\alpha_m - \alpha_n + \alpha_{\max} \\ &= -(\alpha_{\max} - \Delta_m) - (\alpha_{\max} - \Delta_n) + \alpha_{\max} \\ &= \Delta_m + \Delta_n - \alpha_{\max}\end{aligned} \tag{11}$$

where Δ_m and Δ_n are the differences between α_m and $\alpha_{\max}$, and between α_n and $\alpha_{\max}$, respectively. Thus, as long as $\Delta_m + \Delta_n - \alpha_{\max} < 0$ or $\alpha_e < 0$, there will be no negative resistance generated from $\tilde{L}_e$ and, therefore, no instability problem.

A special case is that there is no difference between angles of all main complex inductances. Thus, all main complex inductances share the same complex angle α, which reduce inequality (11) to

$$\alpha_e < -\alpha_{\max} < 0 \tag{12}$$

and thus, no instability problem should appear.

In ordinary cases, the inductive meshes need to be carefully refined to avoid negative resistance. In section A, skin depth

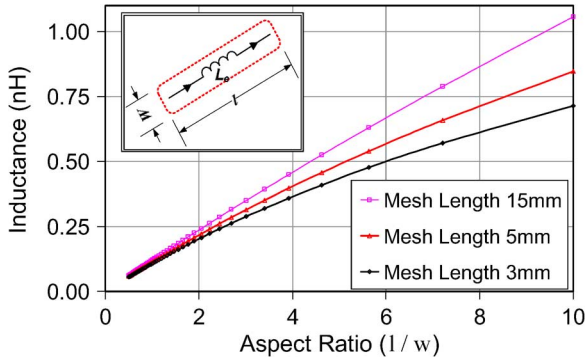

Fig. 4. Main inductance versus aspect ratio of a mesh.

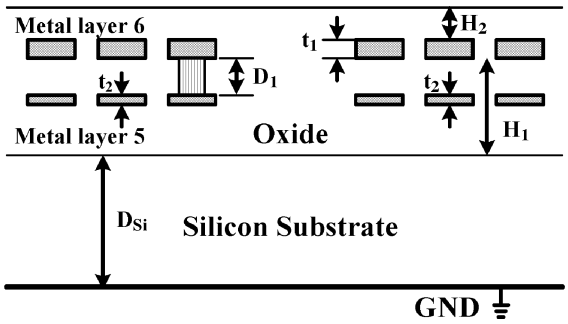

Fig. 5. Cross-sectional view of the fabricated stacked circular inductors.

δ is assumed to be uniform, which makes the conductive loss proportional to the aspect ratio l/w of a mesh, i.e.,

$$\tilde{L} = L - j\frac{1}{\omega\delta\sigma}\frac{l}{w} = |\tilde{L}|e^{-j\alpha}. \tag{13}$$

Fig. 4 shows some typical relations between the main inductance and aspect ratio, which is associated to the conductive loss as given in (13) for some illustrative mesh lengths. The main inductance values are calculated using the formula given in [22].

From Fig. 4, the following can be observed.

- If l is large, the inductance tends to be a linear function of the mesh aspect ratio; hence, the angle differences Δ_m and Δ_n in (11) must approach zero.
- If l is small, the slope of the curve in Fig. 4 becomes smaller as the aspect ratio increases, i.e., the angles of the complex inductances approach $\alpha_{\max}$, which also guarantees that $\alpha_e < 0$.

Once $\alpha_e < 0$, the resistance from the imaginary part of $\tilde{L}_e$ in (10) is guaranteed to be larger than zero, and hence, a physically meaningful DPEC model can be guaranteed. This conclusion can also be further verified by the examples discussed in Section III.

III. Examples

The first two examples presented in this paper are stacked double circular spiral inductors fabricated using a 0.18-μm CMOS process. The cross-sectional view of the fabricated inductor is shown in Fig. 5, where the vertical distance between the double spirals is $D_1 = 0.9$ μm. The upper and lower metal strip thicknesses are $t_1 = 2$ μm and $t_2 = 0.54$ μm, respectively; the height of the metal layer 6 in the oxide substrate is $H_1 = 6.7$ μm and $H_2 = 6$ μm with the relative permittivity

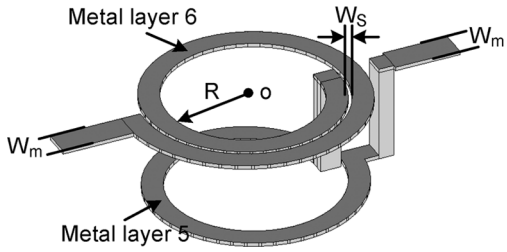

Fig. 6. Geometry of the stacked single circular spiral inductor.

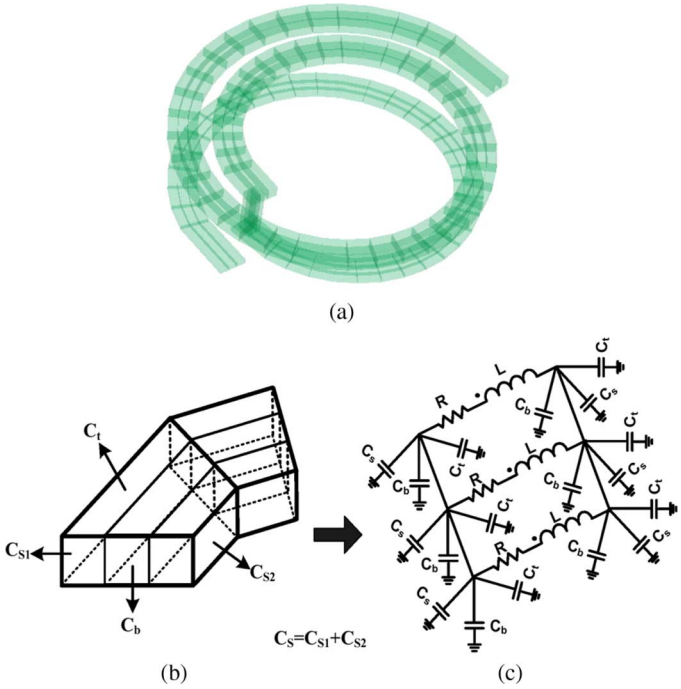

Fig. 7. (a) Capacitive meshes of the inductor shown in Fig. 6. (b) Segment of the meshes. (c) PEEC model of the segment.

$\varepsilon_{\text{oxide}} = 4.0$. The silicon substrate thickness is $D_{\text{Si}} = 350$ μm with the relative permittivity $\varepsilon_{Si} = 11.9$ and the conductivity $\sigma = 10\ \text{S} \cdot \text{m}^{-1}$.

The first example is a stacked single circular spiral inductor. Its geometry is shown in Fig. 6, where the inner radius $R = 44$ μm, the trace width $W_m = 12$ μm, and the trace spacing $W_s = 2$ μm.

The meshing scheme of the structure for the PEEC modeling is shown in Fig. 7(a), where the trapezoid surface cells are for capacitive meshes. The solid inductive cells are half-cell-length shifted from the capacitive cells and are not shown in Fig. 7(a). In Fig. 7(b), C_t, C_b, and C_s represent the capacitances to the ground from the top, bottom, and side surfaces, respectively. The representative PEEC model for a primary section of meshes is shown in Fig. 7(c). All mutual inductance are suppressed in Fig. 7(c) for the purpose of clarity.

Before a DPEC for the inductor was derived, the original PEEC model of this RF inductor had 273 nodes and more than 4000 lumped components. The effective inductance and the Q factor calculated by a DPEC model are compared with those obtained from the measurement in Fig. 8. The threshold value used in this example is 0.15. The result from the original PEEC

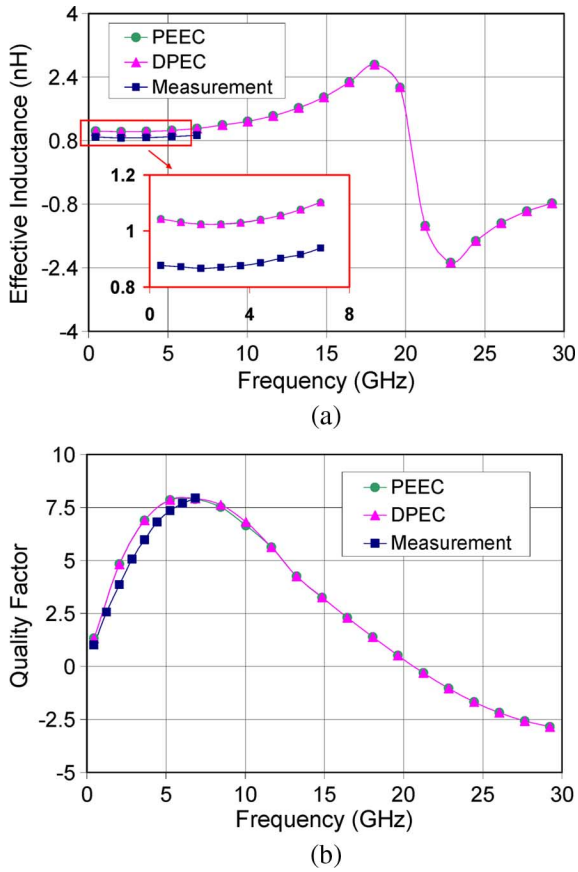

Fig. 8. Characteristics of the stacked single circular spiral inductor by measurement, PEEC and DPEC models. (a) Effective inductance. (b) Q factor.

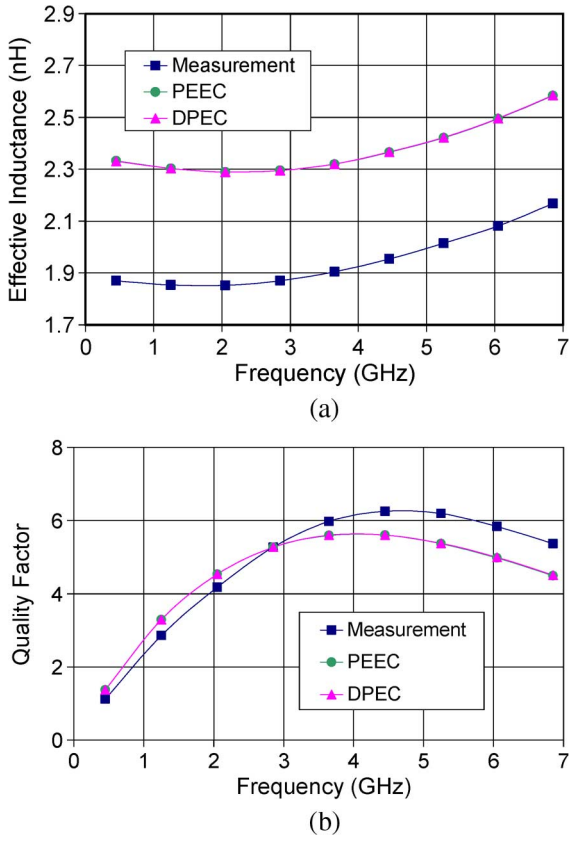

Fig. 10. Characteristics of the stacked double circular spiral inductor by measurement, PEEC, and DPEC models. (a) Effective inductance. (b) Q factor.

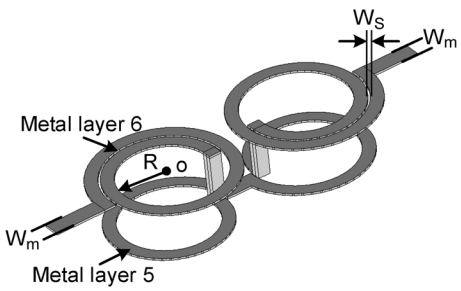

Fig. 9. Geometry of a stacked double circular spiral inductor.

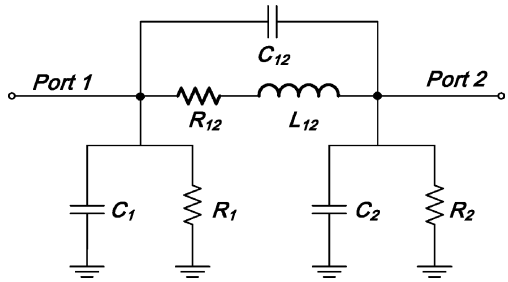

Fig. 11. Obtained DPEC model of the RF inductors.

model is also superimposed as a reference. The definitions of the effective inductance and the Q factor in this study are

$$L = \mathrm{Im}[1/Y_{11}]/\omega \tag{14}$$

$$Q = -\mathrm{Im}[Y_{11}]/\mathrm{Re}[Y_{11}]. \tag{15}$$

The second example is a stacked double circular spiral inductor, as shown in Fig. 9. The original PEEC model for this inductor has 543 nodes and more than 10 000 lumped components.

The effective inductances, as well as the Q factors of the double circular RF inductor from measurement, the original PEEC model, and a DPEC model are shown in Fig. 10.

The final DPEC model for the above two integrated RF inductors can be a three-node network, as shown in Fig. 11. As the circuits are derived at frequencies of interest, there is no approximation error in deriving the DPEC models.

Although the quasi-static Green's functions are used in the PEEC modeling, the L, C, and R values in the DPEC models given here are frequency dependent. Table I lists all the component values at sampled frequencies of each example.

The third example in this study is an LTCC bandpass filter, as depicted in Fig. 12. The filter is with the overall size of 4.9 mm $\times$ 2.36 mm $\times$ 0.55 mm, and consists of four metal layers in the substrate with a 7.8 dielectric constant and 0.002 loss tangent. The metal thickness is 0.012 mm and its conductivity is set to 1×10^7 S $\cdot$ m^{-1} to mimic a real situation if the uneven surface is taken into account. The original PEEC model consists of total 214 nodes. After setting the stopping criteria for $\omega_0^2 \tilde{L}_t \tilde{C}_t$ to 0.15, where ω_0 is the average angular frequency of interest, a DPEC model with only a few nodes can be achieved.

Although all the loss-component values are frequency dependent in principle, in this example, only the loss parameters at the center frequency $f = 2.5$ GHz is used in the analysis and the

TABLE I
COMPONENTS VALUES FOR THE RF INDUCTOR DPEC MODELS

Stacked single circular spiral inductor							
f(GHz)	C_1(fF)	C_2(fF)	C_{12}(fF)	R_1(kΩ)	R_2(kΩ)	R_{12}(Ω)	L_{12}(nH)
0.45	42.09	26.20	46.20	49.40	112.27	2.24	1.046
2.05	33.93	25.92	44.20	6.91	12.35	2.63	1.019
3.65	29.15	23.13	44.77	3.42	4.87	2.96	1.004
5.25	27.87	21.07	45.11	2.41	3.31	3.25	0.995
6.85	23.67	17.47	46.36	1.94	2.60	3.50	0.990
8.45	21.04	15.33	44.23	1.74	2.31	3.74	0.987
10.05	19.44	13.95	43.58	1.65	2.19	3.97	0.985
11.65	18.85	12.99	43.46	1.61	2.16	4.21	0.984
13.25	18.46	12.95	43.85	1.41	1.91	4.46	0.983
14.85	17.81	12.35	43.37	1.39	1.90	4.70	0.982
16.45	17.37	11.90	43.18	1.38	1.92	4.94	0.981
18.05	17.09	11.56	43.31	1.37	1.95	5.28	0.980
19.65	16.93	11.33	43.63	1.34	1.93	5.46	0.979
21.25	16.86	11.18	43.84	1.30	1.90	4.85	0.978
22.85	16.76	11.03	43.94	1.28	1.89	5.08	0.977
24.45	16.84	10.96	44.65	1.18	1.79	5.22	0.977
26.05	16.96	10.87	45.42	1.10	1.70	5.36	0.976
27.65	17.07	10.79	46.26	1.02	1.63	5.49	0.976
29.25	17.19	10.69	47.18	0.94	1.57	5.62	0.976
Stacked double circular spiral inductor							
f(GHz)	C_1(fF)	C_2(fF)	C_{12}(fF)	R_1(kΩ)	R_2(kΩ)	R_{12}(Ω)	L_{12}(nH)
0.45	31.31	32.72	14.48	19.20	15.56	4.80	2.33
1.25	31.19	32.84	13.64	6.88	5.62	5.39	2.29
2.05	31.17	32.88	13.76	4.19	3.43	6.12	2.26
2.85	31.17	32.90	13.85	3.01	2.46	6.86	2.23
3.65	31.17	32.92	13.90	2.35	1.93	7.61	2.22
4.45	31.17	32.95	13.95	1.92	1.58	8.37	2.21
5.25	31.18	32.96	13.97	1.63	1.34	9.13	2.20
6.05	31.20	32.98	13.99	1.41	1.16	9.89	2.19
6.85	31.23	33.00	14.00	1.24	1.02	10.66	2.18

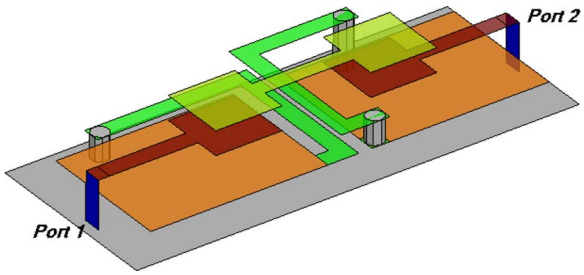

Fig. 12. LTCC bandpass filter.

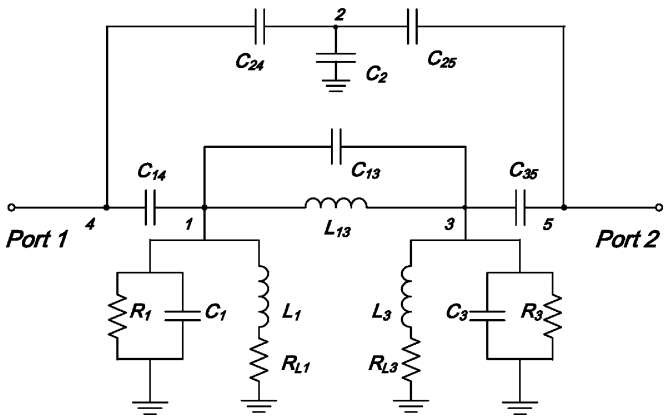

Fig. 13. Obtained six-node DPEC model of the LTCC bandpass filter.

TABLE II
COMPONENTS VALUES FOR THE SIX-NODE DPEC MODEL OF THE BANDPASS FILTER

C_1	2.66 pF	C_{24}	0.40 pF	R_1	10.65 kΩ
C_2	1.80 pF	C_{25}	0.37 pF	R_3	14.492 kΩ
C_3	2.51 pF	L_1	1.41 nH	R_{L1}	0.34 Ω
C_{14}	0.96 pF	L_3	1.52 nH	R_{L3}	0.26 Ω
C_{13}	0.15 pF	L_{13}	6.21 nH		
C_{35}	0.10 pF				

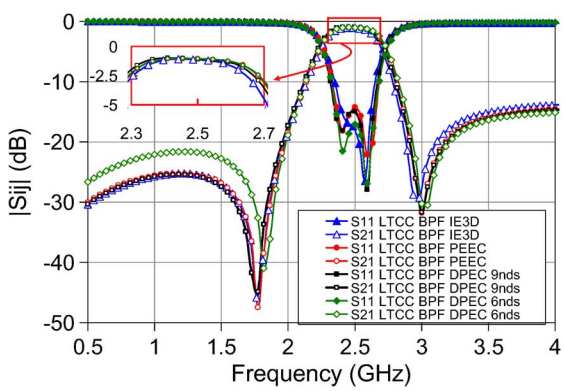

Fig. 14. Magnitudes of S-parameters of the LTCC bandpass filter by IE3D simulation, PEEC model, nine-node DPEC model, and six-node DPEC model.

frequency-independent DPEC model is derived at the center frequency. The DPEC model for the bandpass filter with six nodes is shown in Fig. 13. Note that inductance L_{13} represents the mutual coupling between L_1 and L_3. All the component values in the DPEC model are given in Table II.

The S-parameters of the bandpass filter by the DPEC models with six and nine nodes and those from Zeland Software Inc.'s IE3D [23] have been compared and given in Fig. 14. Good agreement among these results, particularly the insertion loss in the passband that is directly associated to the unloaded Q of the filter, can be observed.

To view the mathematical properties of the circuit system at each step in deriving the DPEC model of the bandpass filter, the poles of the DPEC model at last seven steps for obtaining the six-node DPEC model can be calculated using the modified node analysis [16]. The calculated poles are listed in Table III. For the sake of clarity, the pole's values are normalized to 10^9. The first row of Table III indicates the number of internal nodes that have been reduced, and each column lists the poles sorted by their priority. It can be seen that the imaginary part of the poles represents the loss effect. In a DPEC process, the least important pole is absorbed by the less important poles one by one, whereas the poles with higher priority only change slightly to retain the main physical meanings of the DPEC model. It is interesting to note that the last two reminding poles in Table III represent the two fundamental poles of the two-pole bandpass filter.

It is obvious that, in the above three examples, the DPEC models are capable of retaining the physical properties of the original circuits. Moreover, no negative valued elements are found in the DPEC models, which further justify the rationality of this approach.

TABLE III
SYSTEM POLES OF THE Y-MATRIX FOR THE LTCC BANDPASS FILTER IN DPEC PROCESS. ALL THE NUMBERS ARE NORMALIZED TO 10^9

202nds		203nds		204nds		205nds		206nds		207nds		208nds	
Re.	Im.	Re.	Im.	Re.	Im.	Re.	Im.	Re.	Im.	Re.	Im.	Re.	Im.
0.13	13.87	0.13	13.85	0.13	13.84	0.13	13.83	0.13	13.83	0.13	13.76	0.13	13.70
0.19	16.28	0.19	16.27	0.19	16.25	0.19	16.23	0.19	16.23	0.19	16.19	0.19	16.15
0.37	51.59	0.37	51.60	0.37	51.97	0.37	52.17	0.40	54.26	0.44	59.53		
0.50	66.29	0.50	66.33	0.49	66.47	0.49	66.67	0.49	66.69				
0.98	83.27	0.99	84.33	1.16	94.93	0.76	136.10						
1.35	128.54	1.33	128.58	0.81	139.41								
0.97	139.46	0.98	141.33										
2.76	222.79												

IV. CONCLUSION

In this paper, a new recursive scheme for deriving a succinct DPEC model from a large-scale PEEC model with lossy elements has been proposed. This study is a substantial extension of the original DPEC model for lossless cases proposed by the same research group. In order to deal with the lossy circuit components uniformly, the concept of complex inductance and capacitance has been introduced. The obtained DPEC model not only retains the physical properties of the original PEEC quasi-static electromagnetic model, but also guarantees the passivity of the derived model. In addition to the applications in designing integrated passive circuits on ceramic/organic substrates with loss effects taken into account, this approach can also be applied to the design of RFIC passive elements. Three practical and representative examples have been given to demonstrate the effectiveness and validity of the proposed model.

REFERENCES

[1] A. C. Watson, D. Melendy, P. Francis, K. Hwang, and A. Weisshaar, "A comprehensive compact-modeling methodology for spiral inductors in silicon-based RFICs," *IEEE Trans. Microw. Theory Tech.*, vol. 52, no. 3, pp. 849–857, Mar. 2004.

[2] L. F. Tiemeijer, R. M. T. Pijper, R. J. Havens, and O. Hubert, "Low-loss pattern ground shield interconnect transmission lines in advanced IC processes," *IEEE Trans. Microw. Theory Tech.*, vol. 55, no. 3, pp. 561–570, Mar. 2007.

[3] L. Liang, W.-Y. Yin, and J.-F. Mao, "Implementation of new CMOS differential stacked spiral inductor for VCO design," *IEEE Microw. Wireless Compon. Lett.*, to be published.

[4] L. K. Yeung and K.-L. Wu, "A compact second-order LTCC bandpass filter with two finite transmission zeros," *IEEE Trans. Microw. Theory Tech.*, vol. 51, no. 2, pp. 337–341, Feb. 2003.

[5] K. Nabors and J. White, "FastCap: A multipole accelerated 3-D capacitance extraction program," *IEEE Trans. Comput.-Aided Design Integr. Circuits Syst.*, vol. 10, no. 11, pp. 1447–1459, Nov. 1991.

[6] M. Kamon, M. J. Tsuk, C. Smithhister, and J. White, "Efficient techniques for inductance extraction of complex 3-D geometries," in *IEEE ICCAD'92 Conf. Dig.*, 1992, pp. 438–442.

[7] A. M. Niknejad and R. G. Meyer, "Analysis of eddy-current losses over conductive substrates with applications to monolithic inductors and transformers," *IEEE Trans. Comput.-Aided Design Integr. Circuits Syst.*, vol. 17, no. 4, pp. 305–315, Apr. 1998.

[8] A. M. Niknejad, "Modeling of passive elements with ASITIC," in *IEEE MTT-S Int. Microw. Symp. Dig.*, 2002, vol. 1, pp. 149–152.

[9] Y. Cao, R. A. Groves, X. Huang, N. D. Zamdmer, J.-O. Plouchart, R. A. Wachnik, T.-J. King, and C. Hu, "Frequency-independent equivalent circuit model for on-chip spiral inductors," *IEEE J. Solid-State Circuits*, vol. 38, no. 3, pp. 419–426, Mar. 2003.

[10] N. A. Talwalkar, C. P. Yue, and S. S. Wong, "Analysis and synthesis of on-chip spiral inductors," *IEEE Trans. Microw. Theory Tech.*, vol. 52, no. 2, pp. 176–182, Feb. 2005.

[11] A. Weisshaar, L. Hai, and A. Luoh, "Accurate closed-form expressions for the frequency-dependent line parameters of on-chip interconnects on lossy silicon substrate," *IEEE Trans. Adv. Packag.*, vol. 25, no. 2, pp. 288–296, May 2002.

[12] A. E. Ruehli, "Equivalent circuit models for three-dimensional multiconductor systems," *IEEE Trans. Microw. Theory Tech.*, vol. MTT-22, no. 3, pp. 216–221, Mar. 1974.

[13] D. Melendy and A. Weisshaar, "A new scalable model for spiral inductors on lossy silicon substrate," in *IEEE MTT-S Int. Microw. Symp. Dig.*, Philadelphia, PA, Jun. 2003, pp. 1007–1010.

[14] P. Feldmann and R. W. Freund, "Efficient linear circuit analysis by Padé approximation via the Lanczos process," *IEEE Trans. Comput.-Aided Design Integr. Circuits Syst.*, vol. 14, no. 5, pp. 639–649, May 1995.

[15] K. J. Kerns and A. T. Yang, "Stable and efficient reduction of large, multiport *RC* networks by pole analysis via congruence transformation," *IEEE Trans. Comput.-Aided Design Integr. Circuits Syst.*, vol. 16, no. 7, pp. 734–744, Jul. 1997.

[16] A. Odabasioglu, M. Celik, and L. T. Pileggi, "PRIMA: Passive reduced-order interconnect macromodeling algorithm," *IEEE Trans. Comput.-Aided Design Integr. Circuits Syst.*, vol. 17, no. 8, pp. 645–654, Aug. 1998.

[17] C. P. Yue and S. S. Wong, "Physical modeling of spiral inductors on silicon," *IEEE. Trans. Electron Devices*, vol. 47, no. 3, pp. 560–568, Mar. 2000.

[18] I. Timmins and K.-L. Wu, "An efficient systematic approach to model extraction for passive microwave circuits," *IEEE Trans. Microw. Theory Tech.*, vol. 48, no. 9, pp. 1565–1573, Sep. 2000.

[19] J. Wang and K.-L. Wu, "A derived physically expressive circuit model for multilayer RF embedded passives," *IEEE Trans. Microw. Theory Tech.*, vol. 54, no. 5, pp. 1961–1968, May 2006.

[20] J. R. Mosig, "Arbitrarily shaped microstrip structures and their analysis with a mixed potential integral equation," *IEEE Trans. Microw. Theory Tech.*, vol. 36, no. 2, pp. 314–323, Feb. 1988.

[21] R. Crampagne, M. Ahmadpanah, and J. L. Guiraud, "A simple method for determining the Green's function for a large class of MIC lines having multilayered dielectrics structures," *IEEE Trans. Microw. Theory Tech.*, vol. MTT-26, no. 2, pp. 82–87, Feb. 1978.

[22] C. Hoer and C. Love, "Exact inductance equations for rectangular conductors with applications to more complicated geometries," *J. Res. Nat. Bur. Stand. C*, vol. 69, no. 2, pp. 127–137, Apr.–Jun. 1965.

[23] *"IE3D User's Manual, Release 12,"* Zeland Softw. Inc., Fremont, CA, 2006.

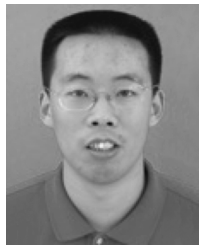

Hai Hu received the B.Sc. degree from Nanjing University, Naning, China, in 2004, and the M.Phil. degree from The Chinese University of Hong Kong, Shatin, Hong Kong, in 2006, both on electronic engineering.

He is currently a Research Assistant with the Department of Electronic Engineering, The Chinese University of Hong Kong. His research interests include computational electromagnetics, CAD, microwave filter synthesis and design, and analysis.

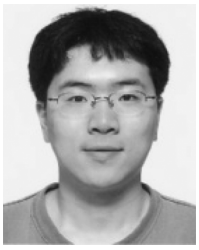

Kai Yang was born in Shanghai, China, in 1982. He received the B.Eng and M.Eng degrees in electronic engineering from Shanghai Jiao Tong University, Shanghai, China, in 2005 and 2008, respectively, and is currently working toward the Ph.D. degree at the University of Texas at Austin.

From 2005 to 2007, he was with the Center for Microwave and RF Technologies at Shanghai Jiao Tong University, Shanghai, China. Since March 2007, he has been a Research Assistant with the Department of Electronic Engineering, The Chinese University of Hong Kong, Shatin, Hong Kong. His current research interests include computational electromagnetics, the design of microwave components, and coupled electromagnetic/circuit simulation.

Ke-Li Wu (M'90–SM'96) received the B.S. and M.Eng. degrees from the Nanjing University of Science and Technology, Nanjing, China, in 1982 and 1985, respectively, and the Ph.D. degree from Laval University, Quebec, QC, Canada, in 1989.

From 1989 to 1993, he was with the Communications Research Laboratory, McMaster University, Hamilton, ON, Canada, as a Research Engineer and a Research Group Manager. In March 1993, he joined the Corporate Research and Development Division, ComDev International, where he was a Principal Member of Technical Staff in charge of developing advanced electromagnetic (EM) design software for passive microwave subsystems for communication satellites. Since October 1999, he has been with the Department of Electronic Engineering, The Chinese University of Hong Kong, Shatin, Hong Kong, where he is currently a Professor. He has authored or coauthored numerous publications in the areas of EM modeling and microwave and antenna engineering. His current research interests include numerical and analytical methods in electromagnetics, passive microwave circuits, filters, antennas for communication systems, LTCC-based multichip modules (MCMs) for wireless communications, and RF identification (RFID) technologies.

Wen-Yan Yin (M'99–SM'01) received the M.Sc. degree in electromagnetic field and microwave technique from Xidian University (XU), Shaanxi, China, in 1989, and the Ph.D. degree in electrical engineering from Xi'an Jiaotong University (XJU), Xi'an, China, in 1994.

From 1993 to 1996, he was an Associate Professor with the Department of Electronic Engineering, Northwestern Polytechnic University (NPU). From 1996 to 1998, he was a Research Fellow with the Department of Electrical Engineering, Duisburg University, granted by the Alexander von Humblodt-Stiftung of Germany. Since December 1998, he has been as a Research Fellow with the MMIC Modeling and Packing Laboratory, Department of Electrical Engineering, National University of Singapore (NUS), Singapore. In March 2002, he joined Temasek Laboratories, NUS, as a Research Scientist and the Project Leader of high-power microwave and ultra-wide band electromagnetic compatibility (EMC)/electromagnetic interference (EMI). From April 2005, he joined the School of Electronic Information and Electrical Engineering, Shanghai Jiao Tong University (SJTU), Shanghai, China, as a Chair Professor in electromagnetic fields and microwave techniques. He is also the Director of the Center for Microwave and RF Technologies, SJTU. He is a reviewer for international journals, including *Radio Science* and *Proceedings of the IEE—Microwave, Antennas, and Propagation*. He is listed as an Editorial Board member and reviewer for the *Journal of Electromagnetic Waves and Applications*. As a lead author, he has authored over 130 international journal papers, including 15 book chapters. One chapter on "Complex Media" is included in the *Encyclopedia of RF and Microwave Engineering* (Wiley, 2005). His main research interests are electromagnetic characteristics of complex media and their applications in engineering, EMC, EMI, and electromagnetic protection, on-chip passive and active MMIC and RFIC device testing, modeling, and packaging, ultra-wideband interconnects and signal integrity, and nanoelectronics.

Dr. Yin was the technical chair of Electrical Design of Advanced Packaging and Systems-2006 (EDAPS'06), technically sponsored by the IEEE Components, Packaging, and Manufacturing Technology (CPMT) Subcommittee. He is a reviewer for five IEEE TRANSACTIONS.